Dalton Transactions

COMMUNICATION

View Article Online
View Journal | View Issue



Cite this: *Dalton Trans.*, 2016, **45**, 9754

Received 21st December 2015,
Accepted 22nd December 2015

DOI: 10.1039/c5dt04960a

www.rsc.org/dalton

# Permanently porous hydrogen-bonded frameworks of rod-like thiophenes, selenophenes, and tellurophenes capped with MIDA boronates†

Peng-Fei Li, Chenxi Qian, Alan J. Lough, Geoffrey A. Ozin and Dwight S. Seferos*

**Permanently porous hydrogen-bonded organic frameworks comprising rod-like molecules with two MIDA boronate termini have been prepared. We show that MIDA boronates self-assemble through multiple hydrogen-bonding interactions. Thiophene-containing frameworks are fluorescent and have a 6.6% absolute quantum yield. The approach appears to be general and introduces new design rules for constructing hydrogen-bonded organic frameworks.**

Porous materials such as metal organic frameworks,[1–3] covalent organic frameworks (COFs),[4–6] and porous aromatic frameworks[7,8] have emerged as promising candidates for a range of uses. Porous organic materials include intrinsic and extrinsic porous structures. Organic cage compounds are a typical class of intrinsic porous crystalline solids.[9–14] Extrinsic porous materials are formed by the assembly of nonporous small molecules including COFs and the recent revival of hydrogen-bonded organic frameworks (HOFs). HOFs are connected by non-covalent interactions such as hydrogen bonds and various π–π interactions. HOFs that incorporate solvent guest molecules typically lose their porosity after the solvent is removed. As a result relatively few HOFs exhibit permanent porosity.[15–22] Permanently porous materials are important for a range of uses,[23–26] yet designing building blocks for permanently porous HOFs is challenging.[15] The most frequently used building blocks contain the 2,4-diaminotriazinyl group (DAT) and related nitrogen-containing heterocycles (Scheme 1).[16] There are a few alternative motifs such as benzimidazolones[18] and pyrazoles,[19] however, the design rules for HOFs are still in their infancy and very important for the continued development of porous materials.

Herein we report that hydrogen-bonded porous frameworks can be constructed from rod-like molecules that are capped with *N*-methyliminodiacetic acid (MIDA) boronate termini. The rod-like molecules contain heterocycles that are typical of optoelectronically active materials, including thiophene, selenophene, and tellurophene.[27–31] The MIDA boronate group has been applied to a range of cross-coupling synthetic methodologies.[32–34] MIDA esters are easily handled, stable under air, and contain both hydrogen bond donors and acceptors. Here we demonstrate that this synthon is useful for the self-assembly of permanently porous materials.

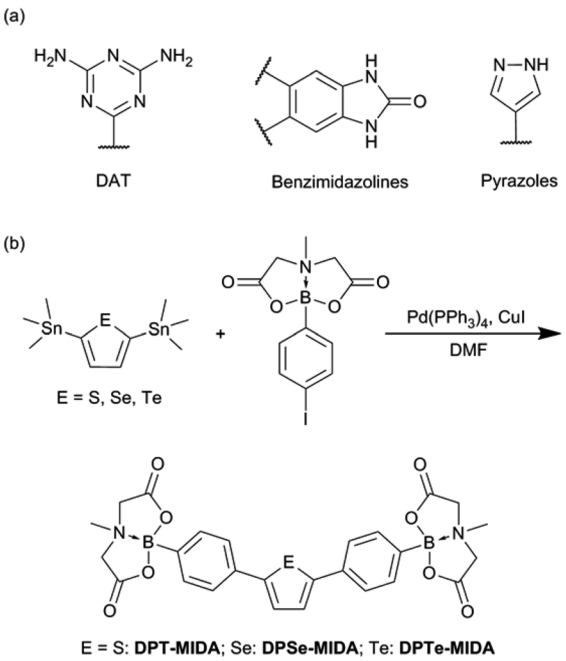


**Scheme 1** (a) Previously reported functional groups for constructing HOFs. (b) The synthesis of diphenylheterocycle MIDA boronates in this report.

MIDA-containing thiophene, selenophene, and tellurophene rod-like molecules (hereafter denoted **DPT-MIDA**, **DPSe-MIDA**, and **DPTe-MIDA**, respectively) were synthesized by a $Pd(PPh_3)_4$ and CuI catalyzed Stille-coupling reaction between

*Department of Chemistry, University of Toronto 80 St. George, Toronto, ON M5S 3H6, Canada. E-mail: dseferos@chem.utoronto.ca*

†Electronic supplementary information (ESI) available: Detailed experimental information and characterization data. CCDC 1434463 (**DPT-MIDA**) and 1434461 (**DPSe-MIDA**). For ESI and crystallographic data in CIF or other electronic format see DOI: 10.1039/c5dt04960a

4-iodophenylboronic acid MIDA ester (3.5 eq.) and the corresponding 2,5-bis(trimethyltin)heterocycle[35,36] (1.0 eq.) (Scheme 1). This reaction afforded yellow solids of **DPT-MIDA**, **DPSe-MIDA**, and **DPTe-MIDA**, respectively in high yields (84%–90%). Pure and crystalline products were obtained by recrystallization from acetonitrile. The MIDA boronates were characterized by FT-IR, NMR, and HR-MS (see the ESI†).

The single crystal structures of **DPT-MIDA** and **DPSe-MIDA** reveal that two molecules of **DPT-MIDA** or **DPSe-MIDA** are contained within each unit cell and the MIDA end groups are in the *trans*-configuration. **DPT-MIDA** crystallize through multiple C–H···O hydrogen bonding and C–H···π interactions (Fig. 1a). The C–H···O hydrogen bonding interactions between the oxygen atom in the carbonyl groups and hydrogen in the methylene groups of adjacent MIDA functionalities vary between 2.20 to 2.65 Å. There are two kinds of C–H···π interactions, one is a 2.85 Å interaction between the thiophene and the phenyl groups of adjacent molecules, the other is a 2.71 Å interaction between the phenyl group and the hydrogen in the methyl group of adjacent MIDA functional groups. **DPSe-MIDA** assembled in a similar fashion (see S4, ESI†). Since the only difference is the chalcogen atom, both of the microporous frameworks have a 7 Å × 10 Å pore size along the shortest distance across the channel. Solvent molecules are incorporated in the channel of the frameworks. Three molecules of acetonitrile are incorporated within the **DPT-MIDA** or **DPSe-MIDA** unit cells. In **DPT-MIDA**, one of the acetonitrile molecule is disordered (see S6, ESI†). In both frameworks, guest acetonitrile molecules are bonded with the wall of the channel through weak C–H···N hydrogen bonding and C–H···π interactions.

**DPTe-MIDA** was also recrystallized from acetonitrile, however only needle-like crystals could be obtained. In order to compare the structure of **DPTe-MIDA** with the other samples, powder X-ray diffraction patterns (PXRDs) were collected on all three compounds. For reference the simulated PXRD patterns of **DPT-MIDA** and **DPSe-MIDA** were generated from their single crystal data. These closely match the experimental PXRD data (see S8–S9, ESI†), indicating that the structure in the powders are similar to the single crystals. The PXRD scattering pattern of **DPTe-MIDA** is weak compared to the other two frameworks, which indicates low crystallinity. None-the-less, the main diffraction peaks are close to the other two frameworks (see S10, ESI†), which implies all three frameworks are assembled into a similar structure.

Thermogravimetric analysis (TGA) was performed on each sample under a $N_2$ atmosphere. These experiments reveal that the incorporated acetonitrile molecules are removed at different temperatures. For S and Se, the guest-removal temperatures are around 150 °C; for Te, the temperature drops to 70 °C (see S11–S13, ESI†). The weight loss of **DPT-MIDA**, **DPSe-MIDA**, and **DPTe-MIDA** are 12%, 8.2%, and 6.1% respectively. This is close to the expected weight loss based on acetonitrile inclusion (10%, 9.4%, and 8.7% for **DPT-MIDA**, **DPSe-MIDA**, and **DPTe-MIDA**, respectively). This provides support that the degree of acetonitrile inclusion is similar in all frameworks. No additional weight loss was observed after the loss of acetonitrile until 350 °C, after which the frameworks began to decompose. The incorporation of acetonitrile in the frameworks was also observed in the $^1$H NMR spectra at $\delta$ = 2.07 ppm (see S14–S16, ESI†).

To investigate stability, variable-temperature PXRD patterns were collected on all three frameworks (Fig. 2 and see S20–S21, ESI†). Under air, structural changes were observed. **DPT-MIDA** is stable up to 100 °C. After that the structure begins to transform, the peaks at 8° and 8.8° become broad, and the peak at 12.2° shifts to 10.7° (Fig. 2). **DPSe-MIDA** is stable in air up to 125 °C. After that the structure begins to transform, the peaks at 5.4°, 8.2°, and 8.8° become broad, the intensity of peak

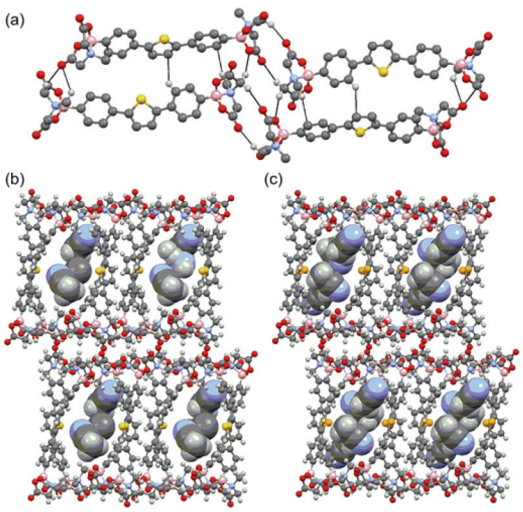


Fig. 1 (a) Hydrogen-bonding interactions in **DPT-MIDA**, (b) and (c) microporous structure of **DPT-MIDA** and **DPSe-MIDA** with acetonitrile solvent incorporated.

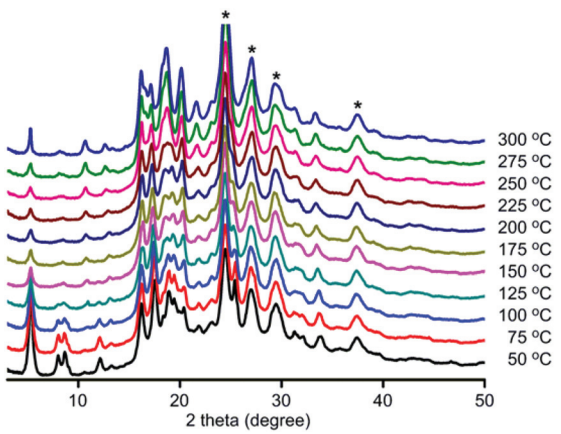


Fig. 2 Variable-temperature PXRD patterns for **DPT-MIDA**. The asterisks (*) denotes the background signal from a polyether ether ketone layer that protects the detector. The temperature was recorded in 25 °C increments.

10.9° increased, while the peak at 12.3° attenuated (see S20, ESI†). Under vacuum, **DPT-MIDA** is stable up to 300 °C (see S22, ESI†). **DPSe-MIDA** is stable under vacuum as well, even when heated at 150 °C overnight, no obvious change was observed using optical microscopy (see S24, ESI†). Thermally induced transformation are difficult to observe for **DPTe-MIDA** due to the lower diffraction intensity of this less crystalline sample.

Permanent porosity was evaluated by $CO_2$ adsorption at 273 K. Activated frameworks have 267, 239 and 197 $m^2\ g^{-1}$ BET surface areas for **DPT-MIDA**, **DPSe-MIDA**, and **DPTe-MIDA**, respectively. The surface area decreases with the increase in molecular weight, which is another sign of similar structure. A slight deviation from linearity is observed which could come from larger atomic radii and lower crystallinity of the Te frameworks (see S25, ESI†). The pore width distributions of **DPT-MIDA** and **DPSe-MIDA** have a peak at 5 Å, which is slightly smaller than the pore width expected from single crystal data, likely due to lattice shrinkage after solvent removal (see S26–S27, ESI†). For **DPTe-MIDA**, two peaks are observed, one at 5.5 Å, and one at 9.8 Å (see S28, ESI†). While the peak at 5.5 Å comes from the ideal crystal structure, the peak at 9.8 Å is almost twice as large and likely come from molecular vacancies in the lattice. **DPT-MIDA** and **DPSe-MIDA** take up 39 and 36 $cm^3\ g^{-1}$ of $CO_2$ (STP), which corresponds to 1 mole of $CO_2$ adsorbed per mole of building block. **DPTe-MIDA** takes up 15 $cm^3\ g^{-1}$ (STP) of $CO_2$, corresponds to around 0.5 mole of $CO_2$ adsorbed per mole of building block (Fig. 3).

Since thiophene, selenophene, and tellurophene are incorporated into the frameworks, it is interesting to examine their optical properties. The solution absorption maximum ($\lambda_{max}$) of the solvated molecules shifts to longer wavelengths (lower energy) as one moves from S (334 nm) to Se (344 nm) to Te (356 nm) in acetonitrile. The emission spectra also red shift from S (412 nm) to Se (424 nm) to Te (439 nm) (see S29–S30, ESI†). The absolute quantum yield of the solid was measured using an integrating sphere.[37] Here we chose to focus on **DPT-MIDA** because it exhibits the strongest fluorescence in solution. The absolute quantum yield of **DPT-MIDA** is 6.6%. This value is quite high for HOFs and greater than both **HOF-1111**[38] and **HOF-5**,[22] which undergo aggregation induced emission. A powder of **DPT-MIDA** exhibits strong enough blue fluorescence that can be observed with the naked eye (see S31, ESI†).

In conclusion, we have discovered that rod-like molecules that possess two MIDA boronate termini self-assemble into permanently porous HOFs. The thiophene-containing framework exhibits strong photoluminescence in the solid state. Combining rod-like molecules and MIDA esters appears to be a straightforward way to develop porous solids and could be quite general for other types of building blocks with a variety of shapes and symmetry. Thus the design rules presented herein should be useful for new types of frameworks for a range of uses.

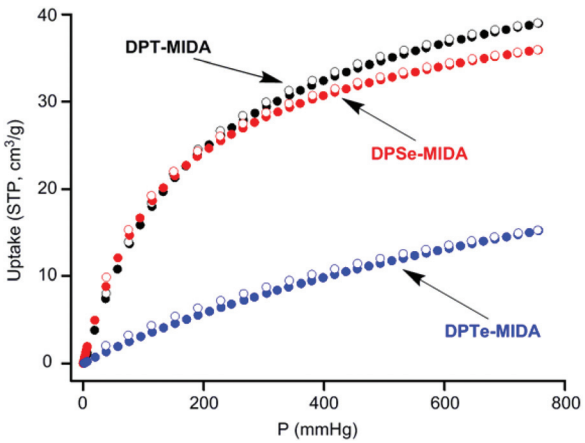


Fig. 3 $CO_2$ sorption isotherm of **DPT-MIDA**, **DPSe-MIDA** and **DPTe-MIDA** at 273 K. (filled circles: adsorption, open circles: desorption, STP = standard temperature pressure).

## Acknowledgements

This work was supported by the National Science and Engineering Research Council of Canada and the Alfred P. Sloan Foundation. GAO is Government of Canada Research Chair in Materials Chemistry and Nanochemistry.

## Notes and references

1 M. Eddaoudi, D. B. Moler, H. Li, B. Chen, T. M. Reineke, M. O'Keeffe and O. M. Yaghi, *Acc. Chem. Res.*, 2001, **34**, 319–330.
2 O. M. Yaghi, M. O'Keeffe, N. W. Ockwig, H. K. Chae, M. Eddaoudi and J. Kim, *Nature*, 2003, **423**, 705–714.
3 M. O'Keeffe, M. A. Peskov, S. J. Ramsden and O. M. Yaghi, *Acc. Chem. Res.*, 2008, **41**, 1782–1789.
4 M. Mastalerz, *Angew. Chem., Int. Ed.*, 2008, **47**, 445–447.
5 X. Feng, X. Ding and D. Jiang, *Chem. Soc. Rev.*, 2012, **41**, 6010–6022.
6 S.-Y. Ding and W. Wang, *Chem. Soc. Rev.*, 2013, **42**, 548–568.
7 N. B. McKeown and P. M. Budd, *Chem. Soc. Rev.*, 2006, **35**, 675–683.
8 D. Wu, F. Xu, B. Sun, R. Fu, H. He and K. Matyjaszewski, *Chem. Rev.*, 2012, **112**, 3959–4015.
9 T. Tozawa, J. T. A. Jones, S. I. Swamy, S. Jiang, D. J. Adams, S. Shakespeare, R. Clowes, D. Bradshaw, T. Hasell, S. Y. Chong, C. Tang, S. Thompson, J. Parker, A. Trewin, J. Bacsa, A. M. Z. Slawin, A. Steiner and A. I. Cooper, *Nat. Mater.*, 2009, **8**, 973–978.
10 J. T. A. Jones, T. Hasell, X. Wu, J. Bacsa, K. E. Jelfs, M. Schmidtmann, S. Y. Chong, D. J. Adams, A. Trewin, F. Schiffman, F. Cora, B. Slater, A. Steiner, G. M. Day and A. I. Cooper, *Nature*, 2011, **474**, 367–371.

11 T. Hasell, S. Y. Chong, K. E. Jelfs, D. J. Adams and A. I. Cooper, *J. Am. Chem. Soc.*, 2012, **134**, 588–598.
12 M. W. Schneider, I. M. Oppel, A. Griffin and M. Mastalerz, *Angew. Chem., Int. Ed.*, 2013, **52**, 3611–3615.
13 L. Chen, P. S. Reiss, S. Y. Chong, D. Holden, K. E. Jelfs, T. Hasell, M. A. Little, A. Kewley, M. E. Briggs, A. Stephenson, K. M. Thomas, J. A. Armstrong, J. Bell, J. Busto, R. Noel, J. Liu, D. M. Strachan, P. K. Thallapally and A. I. Cooper, *Nat. Mater.*, 2014, **13**, 954–960.
14 G. Zhang, O. Presly, F. White, I. M. Oppel and M. Mastalerz, *Angew. Chem., Int. Ed.*, 2014, **53**, 1516–1520.
15 J.-H. Fournier, T. Maris and J. D. Wuest, *J. Org. Chem.*, 2004, **69**, 1762–1775.
16 Y. He, S. Xiang and B. Chen, *J. Am. Chem. Soc.*, 2011, **133**, 14570–14573.
17 A. I. Cooper, *Angew. Chem., Int. Ed.*, 2012, **51**, 7892–7894.
18 M. Mastalerz and I. M. Oppel, *Angew. Chem., Int. Ed.*, 2012, **51**, 5252–5255.
19 T.-H. Chen, I. Popov, W. Kaveevivitchai, Y.-C. Chuang, Y.-S. Chen, O. Daugulis, A. J. Jacobson and O. Š. Miljanić, *Nat. Commun.*, 2014, **5**, DOI: 10.1038/ncomms6131.
20 P. Li, Y. He, H. D. Arman, R. Krishna, H. Wang, L. Weng and B. Chen, *Chem. Commun.*, 2014, **50**, 13081–13084.
21 W. Xiao, C. Hu and M. D. Ward, *J. Am. Chem. Soc.*, 2014, **136**, 14200–14206.
22 H. Wang, B. Li, H. Wu, T.-L. Hu, Z. Yao, W. Zhou, S. Xiang and B. Chen, *J. Am. Chem. Soc.*, 2015, **137**, 9963–9970.
23 Y. Kou, Y. Xu, Z. Guo and D. Jiang, *Angew. Chem., Int. Ed.*, 2011, **50**, 8753–8757.
24 Y. Li, S. Zhang and D. Song, *Angew. Chem., Int. Ed.*, 2013, **52**, 710–713.
25 M. G. Campbell, D. Sheberla, S. F. Liu, T. M. Swager and M. Dincă, *Angew. Chem., Int. Ed.*, 2015, **54**, 4349–4352.
26 P.-F. Li, T. B. Schon and D. S. Seferos, *Angew. Chem., Int. Ed.*, 2015, **54**, 9361–9366.
27 J. Hollinger, A. A. Jahnke, N. Coombs and D. S. Seferos, *J. Am. Chem. Soc.*, 2010, **132**, 8546–8547.
28 A. A. Jahnke, G. W. Howe and D. S. Seferos, *Angew. Chem., Int. Ed.*, 2010, **49**, 10140–10144.
29 L. Li, J. Hollinger, A. A. Jahnke, S. Petrov and D. S. Seferos, *Chem. Sci.*, 2011, **2**, 2306–2310.
30 G. L. Gibson, T. M. McCormick and D. S. Seferos, *J. Am. Chem. Soc.*, 2012, **134**, 539–547.
31 Y. S. Park, Q. Wu, C.-Y. Nam and R. B. Grubbs, *Angew. Chem., Int. Ed.*, 2014, **53**, 10691–10695.
32 E. P. Gillis and M. D. Burke, *J. Am. Chem. Soc.*, 2008, **130**, 14084–14085.
33 J. Li, S. G. Ballmer, E. P. Gillis, S. Fujii, M. J. Schmidt, A. M. E. Palazzolo, J. W. Lehmann, G. F. Morehouse and M. D. Burke, *Science*, 2015, **347**, 1221–1226.
34 P. Trinchera, V. B. Corless and A. K. Yudin, *Angew. Chem., Int. Ed.*, 2015, **54**, 9038–9041.
35 D. P. Sweat and C. E. Stephens, *Synthesis*, 2009, 3214–3218.
36 T. Earmme, Y.-J. Hwang, N. M. Murari, S. Subramaniyan and S. A. Jenekhe, *J. Am. Chem. Soc.*, 2013, **135**, 14960–14963.
37 D. O. Faulkner, J. J. McDowell, A. J. Price, D. D. Perovic, N. P. Kherani and G. A. Ozin, *Laser Photon. Rev.*, 2012, **6**, 802–806.
38 Z. Sun, Y. Li, L. Chen, X. Jing and Z. Xie, *Cryst. Growth Des.*, 2015, **15**, 542–545.